Passive control of cavity acoustics via the use of surface waviness at subsonic flow

Journal:	*Aircraft Engineering and Aerospace Technology*
Manuscript ID	AEAT-01-2018-0061.R1
Manuscript Type:	Research Paper
Keywords:	Aeroacoutics, Landing Configurations, Cavity Noise, Surface waviness, OpenFOAM

Passive control of cavity acoustics via the use of surface waviness at subsonic flow

Abstract

Purpose – Aircraft noise is dominant for residents near airports when planes fly at low altitudes such as during departure and landing. Flaps, wings, landing gear contribute significantly to the total sound emission.

This paper aims to present a passive flow control (in the sense that there is no power input) to reduce the noise radiation induced by the flow over the cavity of the landing gear during take-off and landing.

Design/methodology/approach – The understanding of the noise source mechanism is normally caused by the unsteady interactions between the cavity surface and the turbulent flows as well as some studies have shown tonal noise due to cavity resonances, this tonal noise is dependent on cavity geometry and incoming flow, lead us to use of a sinusoidal surface modification application upstream of a cavity as a passive acoustics control device in approach conditions.

Findings – It is demonstrated that the proposed surface waviness showed a potential reduction in cavity resonance and in the overall sound pressure level at the majority of the points investigated in the low Mach number. Furthermore, optimum sinusoidal amplitude and frequency were determined by the means of a two-dimensional Computational Fluid Dynamics analysis for a cavity with a length to depth ratio of 4.

Research limitations/implications – The noise control by surface waviness has not implemented in real flight test yet, as all the tests are conducted in the credible numerical simulation.

Practical implications –. The application of passive control method on the cavity requires a global aerodynamic study of the airframe is a matter of ongoing debate between aerodynamicists and acousticians. The latter is aimed at the reduction of the noise whereas the former fears a corruption of flow conditions. In order to balance aerodynamic performance and acoustics, the use of the surface waviness in cavity leading edge is the most optimal solution.

Social implications – The proposed leading edge modification it has important theoretical basis and reference value for engineering application it can meet the demands of engineering practice. Particularly, to contribute to the reduce the aircraft noise adopted by the “European Visions 2020”.

Originality/value – The investigate cavity noise with and without surface waviness generation and propagation by employing a hybrid approach, the computation of flow based on the Large-eddy simulation (LES) method, is decoupled

from the computation of sound, which can be performed during a post-processing based on Curle's acoustic analogy as implemented in OpenFOAM.

Keywords Aeroacoutics, Landing Configurations, Cavity Noise, Surface waviness, OpenFOAM.

Paper type: Research paper.

1 Introduction

Airframe noise refers to the noise generated by all components of the aircraft except the propulsion system. With the implementation of quieter jet propulsion systems, airframe noise becomes especially significant for larger, modern commercial aircraft. Moreover, the environmental regulations are concerned with the noise levels at and around airports during the take-off and landing situations. The international civil aviation organization (ICAO) annex 16 is the one involved with setting the standards of noise levels for aircraft and engine manufacturers. Thus, the radiation of airframe noise will be a necessary component of the development of future commercial aircraft, particularly in the subsonic fleet. Earlier investigations indicated that there are many sources that contribute to airframe noise. One such component is cavity noise. Flow over cavities on solid surfaces became a topic of interest in the late 1950s and early 1960s with the introduction of high speed combat aircraft. The primary concerns at that time were the buffeting of the cockpits and the drag induced by flow over bomb bays and landing gear compartments, Figure 1.

Figure 1 Bomb bays and landing gear.

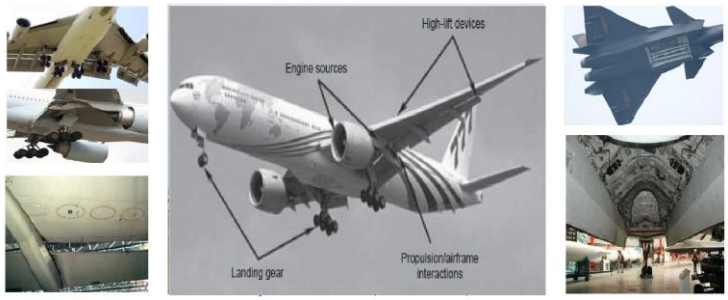

2 Control of Cavity Noise

Many control techniques have been tested in order to reduce the cavity acoustic tones with variable results. Both active and passive control systems have been used. Passive control devices are the easiest to implement and a wide variety of systems were tested, in particular: spoilers, mass injection and modification of the cavity leading and/or trailing edge. These concepts sometimes proved to be very effective in reducing energetic tones.

The effect of a waviness surface in incompressible cross flow parallel to the leading edge of the cavity is another passive device that proved to be very efficient, as shown first by Garry Hughes and Laurent Dala (GARRY, DALA, 2009).

3 Investigation of Flow Phenomena for Cavity Flow

3.1 Cavity Geometry

Figure 2-(a) illustrates the length L, depth D and width W with the stream wise flow direction and the Figure 2-(b) carries details showing the incoming boundary layer at the leading edge of the cavity, shear layer over the cavity and the pressure perturbation from the trailing edge of the cavity due to the impingement of the shear layer on the corner of the downstream of the cavity. Cavities can be classified based on the geometrical rations of the length to depth (L/D).

Figure 2 Cavity dimensions and flow characteristics

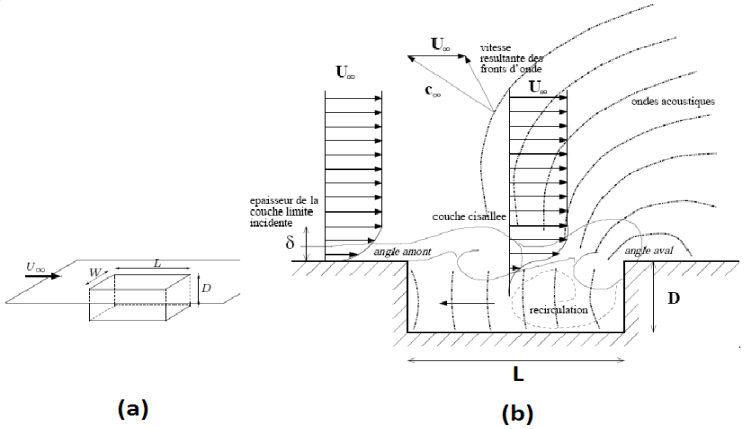

Ratio of Length over Depth L/D: Cavity flows exhibit a wide variety of phenomena whose precise nature depends sensitively on a number of parameters including the value of L/D. In the literature, vastly different values of L/D have been quoted to define the flow types. For instance: L/D < 7 for open and L/D > 13 for closed cavity flow is reported by Stallings and Wilcox (Stallings et al.,1987) whereas L/D < 10 for open and L/D > 13 for closed cavity flow is reported in the work of Plentovich (Plentovich, 1992). Similarly, (Dix et al., 2000) quote L/D < 9 for open and L/D > 13 for closed cavity flow whereas (Srinivisan et al.,1991) quote L/D < 3 for open and L/D > 10 for closed cavity flow fields. Tracy and Plentovich (Tracy et al.,1992) investigated the variations in the values of L/D and concluded that the vast disagreements in the literature were due to the dependence of the cavity flow type on Mach number as well as L/D. Figure 3-(b) shows separation point at the upstream of the cavity and stagnation point at the downstream of the cavity with dividing streamline for the open cavity at subsonic velocity. For the closed cavity at the subsonic speed Figure 3-(c), a separation point occurs at the leading edge of the cavity, impingement point and second separation point are at the bottom of the cavity with a stagnation point at the trailing edge of the cavity. In the closed cavity configuration, the profile of the dividing stream line starts from the bottom of the cavity.

Open cavities refer to flow over cavities where the boundary layer separates at the upstream corner and reattaches near the downstream corner. Open cavities may further be divided into shallow and deep cavities. The cavities with aspect ratio $L/D>1$ may considered as shallow and $L/D<1$ for the cavities may be considered deep Figure 3-(a). Cavities are

closed when the separated layer reattaches at the bottom of the cavity and again separates ahead of the downstream wall of the cavity.

Figure 3 Schematic of deep (a), and shallow cavities: open (b), and closed (c)

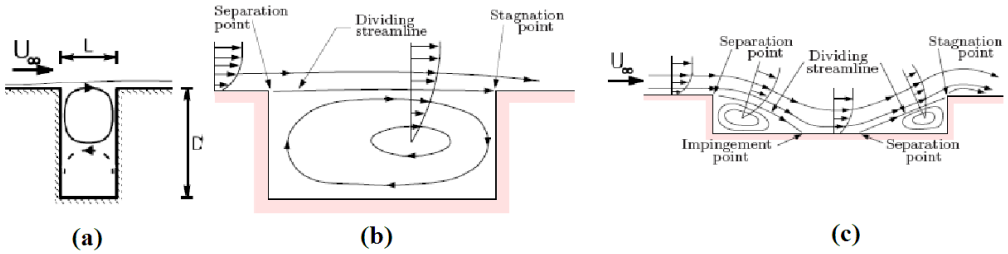

3.2 Incoming Flow

The influence of the free stream flow velocity has been investigated in the majority of the experimental studies. The cavity flow physics and its resonance depend on several flow parameters.

Mach Number

The effects of Mach number on non-dimensional frequency fb/U_e have been studied by many investigations for both laminar and turbulent boundary layers. On the basis of high speed shadow-graphs of cavity oscillation, (Rossiter,1964) speculated that periodic vortices are shed at the upstream corner in sympathy with the pressure oscillation produced by interaction of the vortices with the downstream corner. Based on this idea Rossiter derived a formula for the oscillation frequency. Heller and Covert (Heller et al., 1971) studied shallow cavities over a wide range of Mach numbers and correlated a great many experimental results with Rossiter's formulation of cavity oscillation frequency, the vortices shed from the upstream cavity corner are assumed to convect at a constant phase velocity through the shear layer, resulting in a linear phase distribution. The variation in the resonant frequencies with Mach number is consistent with the Rossiter Eqn. (1).

Boundary Layer Thickness

The boundary layer thickness at the cavity lip is also an important parameter (Ahuja et al., 1995). Colonius (Colonius, 2004) states that the momentum thickness θ_0 at the leading edge of the cavity plays a vital role in the selection of the modes and in governing the growth of the shear layer. They also found L/θ for lower limit for the cavity resonance to be approximately $L/\theta \approx 80$. When the ratio of the cavity length to the momentum thickness of the incoming boundary layer (L/θ) is in the range 80 < L/θ< 120, the self-sustained oscillations take place in the shear layer mode. When L/θ exceeds 120, another mode of cavity oscillation has been observed, but has received much less attention, and is relatively poorly understood. In incompressible experiments for an axisymmetric cavity, Gharib and Roshko (Gharib et al.,1987) observed a wake mode, where the oscillating flow over the cavity resembles the wake behind a bluff body, rather

than a free shear layer. Flow features in this wake mode were qualitatively very different from those in the shear-layer mode described by Rossiter, and wake mode was accompanied by a large increase in drag. Similar dramatic increases in drag had been previously observed by Fox (Fox,1968) as the cavity length was increased, in flows with thin laminar upstream boundary layers, and Roshko (Roshko, 1955) observed an intermittency analogous to the large fluctuations of drag which occur on a bluff cylinder in the critical range of Reynolds number, where the flow may be switching between shear-layer mode and a type of wake mode.

Sarohia (Sarohia, 1975) stated that the parameters cavity depth D and initial momentum thickness θ_0 at the leading edge also are as important as the cavity length L, for a fixed value of the edge velocity U_e, depth D and Width W, there exists a maximum value of shear thickness above which the cavity does not oscillate. As the shear layer thickness δ_0 is decreased ($\delta_0 < \delta_{0_{max}}$), the frequency of cavity oscillations increases.

3.3 Flow Models

Rossiter In 1964, proposed a semi-empirical formula for predicting the discrete tones detected in the experiments. The vortices which are shed from the cavity leading edge are convected downstream until they interact with the aft cavity wall, generating acoustic pulses. These acoustic pulses propagate upstream in the cavity eventually reaching the front cavity wall. At this time they induce separation of the shear layer which results in the shedding of another vortex, completing the feedback loop. Based on this description a formula was proposed to predict the frequencies, given by Eqn. (1):

$$f_m = \frac{U_\infty}{L}\frac{m-\gamma}{M_\infty + \frac{1}{\kappa}} \tag{1}$$

Where m is an integer index for the frequency of interest (m=1, 2, 3...), is constant for a fixed L/D and κ represents the ratio of the speed of the vortices to the free-stream speed.

The Figure 4 illustrate typical spectra for cavity with open flow as well as a section of the resonant range classification presented in (Plentovich,1993) corresponding to the cavity dimensions of interest for this study.

Where κ is empirical constant, $\kappa = 0.57$ yields a fairly good collapse with the experimental data. For shallower cavities (L/D from 4 to 10), Rossiter adjusted the constant, by using the values of Table.1.

Table 1. Values of γ as a function of the length-to-depth ratio L/D, from (Rossiter,1964)

L/D	γ
4	0.25
6	0.38
8	0.54
10	0.58

Figure 4 Typical Spectral View of Rossitor Modes (Plentovich,1992)

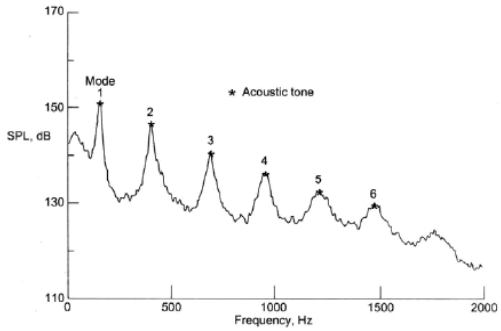

The acoustic waves generated at the downstream corner will induce the shedding of vortices at the upstream corner. This vorticity is in turn responsible for the acoustic emission as it interacts with the downstream corner. λ_a denotes the acoustic wavelength and λ_v the aerodynamic wavelength, that is the spacing between two vortices. At the initial time t = 0, the phase of the upstrem-propagating acoustic wave is supposed to be zero, and the cavity spans n_a complete wavelengths λ_a. At this time, there is a vortex located at a distance $\alpha_v\lambda_v$ downstream of the downstream corner, as depicted in Figure 5 (a).

Figure 5. Simplified model of the flow over a cavity

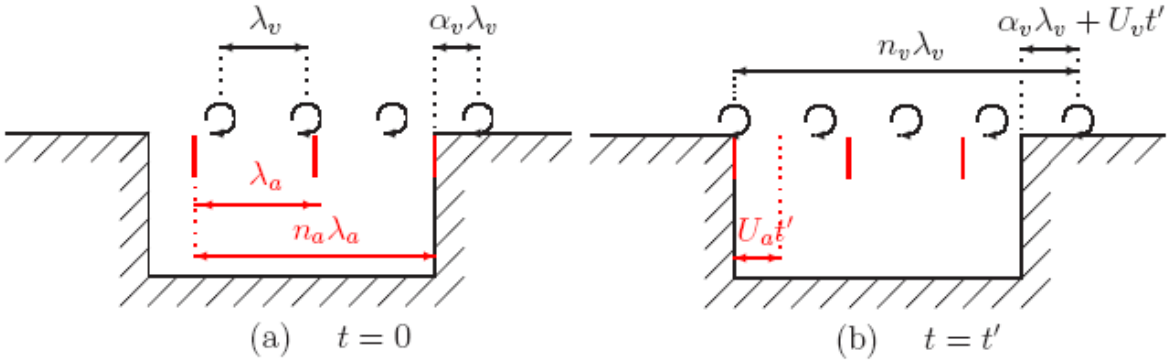

At the time $t = t'$, a wavefront reaches the upstream corner, synchronized with the shedding of a new vortex. The vortices have been convected over a distance $U_v t'$, and the vortex downstream of the downstream corner is now located at $\alpha_v\lambda_v + U_v t'$, as indicated in (figure 5 (b)). For the n_v vortices above the cavity opening, we can write Eqn. (2):

$$n_v\lambda_v = L + \alpha_v\lambda_v + U_v t' \quad (2)$$

In the same period of time, the acoustic wavefronts have propaged over $U_a t'$ in the supstream direction, so that Eqn. (3):

$$L = \alpha_a\lambda_a + U_a t' \quad (3)$$

Eliminating t', this yields:

$$\frac{U_v}{U_a} n_a\lambda_a + (n_v - \alpha_v)\lambda_v = L\left(1 + \frac{U_v}{U_a}\right) = kL\left(\frac{1}{k} + M\frac{c_\infty}{U_a}\right) \quad (4)$$

where c_∞ is the sound speed above the cavity, k is the ratio $\frac{U_v}{U_\infty}$, and M the Mach number $\frac{U_\infty}{c_\infty}$. The oscillation frequency $f = \frac{U_v}{\lambda_v} = \frac{U_a}{\lambda_a}$ is introduced to lead:

$$\frac{fL}{U_\infty} = \frac{(n_a + n_v - \alpha_v)}{\left(\frac{1}{k} + M\frac{c_\infty}{U_a}\right)} \quad (5)$$

A comparison with the empirical Eqn (1) indicates that the physical model is compatible with the experimental data if we choose: $n_v + n_a = m$; $\alpha_v = \alpha$; $K = k$; $c_\infty = U_a$.

Bilanin and Covert's In 1973, this analysis consists of three parts: the analysis of the shear layer stability: the calculation of the interior acoustics of a rectangular cavity; and the prediction of the cavity oscillation frequency. In the first part of the calculation, the shear layer is modeled as a vortex sheet that is only dependent upon the depth of the cavity. With this assumption, the effect of shear layer impingement at the downstream edge of the cavity is eliminated, and the separation of upstream and downstream edge effects and the pressure field from the upstream edge have little effect on the vortex sheet except near the upstream edge.

Therefore, the only boundary conditions required in the stability analysis are the rigid wall boundary condition at the floor of the cavity, the kinematic and dynamic boundary conditions at the shear layer interface, and the outgoing radiation boundary condition above the shear layer. According to the photographs taken by Krishnamurty (Krishnamurty, 1955), the shear layer impingement generates an acoustic source at the downstream edge of the cavity. Hence, in the second part of the analysis, Bilanin and Covert (Bilanin et al., 1973) assumed a mass addition and removal at the downstream edge of the cavity as the cause of the acoustic source. The following expression is derived:

$$St = \frac{n - \frac{3}{8} - \frac{\phi}{2\pi}}{\frac{\alpha_r U_\infty}{\omega} + M\frac{c_+}{c_-}} \quad (6)$$

Where ϕ and $2\pi \times 3/8$ correspond to the phase lags, respectively due to the upstream and downstream edges, ω and α_r are the radian frequency and the real part of the complex wavenumber of the unstable vortex sheet solution respectively and U_∞ is the velocity outside the cavity. This formula takes the compressibility factor into account through the ratio c_+/c_- between the exterior and interior sound speeds.

In the study by Bilanin and Covert, the internal cavity wave structure is uncoupled from the shear layer motion in order to simplify the analysis. It is assumed that the cavity internal pressure modes force the shear layer only at the upstream edge and, therefore, only the downstream wave motion of the shear layer is considered. To eliminate this assumption, Heller and Bliss (Heller et al., 1975) introduced the concept of the pseudopiston effect Figure 6 (Rockwell et al., 1980).

Figure 6 Classes of possible of vortex-corner interactions.
From (Rockwell et al., 1980)

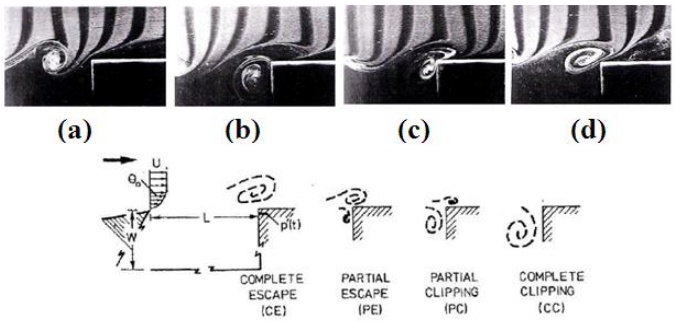

This is similar to the replacement of the downstream cavity wall with an oscillating piston. The mass addition and removal creates pressure fluctuations that travel upstream in the cavity, and further amplifies the vortices shed at the upstream edge. In this manner, the internal cavity acoustic wave is coupled with the shear layer motion, and the feedback loop is complete.

4 Acoustic Analogies

Modern aeroacoustic science was pioneered in the 1950's by Sir James Lighthill (Lighthill ,1952) who derived an 'acoustic analogy' for the estimation of the intensity of sound radiated by a turbulent flow. Lighthill transformed the Navier-Stokes and continuity equations to form an exact, inhomogeneous wave equation whose source terms are important only within the turbulent region.

4.1 Lighthill's acoustic analogy

Lighthill gives a reformulation of the fluid dynamics equations in such a way that he obtains a wave equation for the acoustic density fluctuations with a source term on the right hand side. The following equation is obtained:

$$\frac{\partial^2 \rho}{\partial t^2} - C_0^2 \Delta \rho = -\frac{\partial^2 T_{ij}}{\partial X_i \partial X_j} \tag{7}$$

Where ρ is the density, C_0 is the ambient sound speed and $\mathrm{T_{ij}} = \rho \mathrm{u_i u_j} + \left(\mathrm{P} - \mathrm{c_0^2}\rho\right)\delta_{\mathrm{ij}} - \tau_{\mathrm{ij}}$ is known as the Lighthill stress tensor, $\mathrm{u_i}$ p, τ_{ij} being the velocity components, the pressure and the viscous stresses respectively.

4.2 Curle's Analogy: the influence of solid boundaries

As an extension to Lighthill's acoustic analogy, Curle (Curle, 1955) proposed a formal solution to Lighthill's analogy in 1955 to include the influence of the solid static boundaries. The presence of surfaces strongly modify the sound production:

- Changes in the radiated acoustic field in comparison with the previous case of free turbulent flows;
- Extension of the integral formulation to the case of wall-bounded turbulent flows;

We assume a solid body, placed normally to a mean flow: The volume V is the entire space occupied by the fluid, and V is delimited by a surface S enclosing the body. $\vec{n}$ is the outer normal to the volume V at the surface S, directed towards the body.

$$\rho(\vec{x},t)=\frac{x_i x_j}{4\pi c_0^4|\vec{x}|^3}\frac{\partial^2}{\partial t^2}\int\int_V\int\left[T_{ij}\right]d\vec{y}-\iint_S\frac{1}{4\pi c_0^2|\vec{x}|}\frac{\partial}{\partial t}\left[\rho u_i\right]n_i dS-\frac{x_j}{4\pi c_0^3|\vec{x}|^2}\frac{\partial}{\partial t}\iint_S\left[\rho u_i u_j+p\delta_{ij}-\tau_{ij}\right]n_i ds \quad (8)$$

- The first integral (volumic integral) represents the noise due to the turbulence in the source volume, similarly to the case of a free turbulent flow;
- The second integral (surfacic integral) results from a volume injection through the surface S enclosing the body, which can be due to a flow through a porous surface or to pulsations of the body;
- The third integral (surfacic integral) results from the momentum flux through the surface S and from the surface stresses on S (pressure and viscosity forces);

5. Large Eddy Simulations

The solver use traditional Large Eddy Simulations (**LES**) wall model in conjunction with an acoustic analogy, in order to predict the aeroacoustic behavior of cavity flow. The idea underlying LES is so called convergent evolution. Behavior of the large-scale eddies depends strongly on the forces acting on the flow and on initial and boundary conditions; they are flow-dependent. Small-scale eddies are generally in dependent from what is happening on the larger scales; they are flow-independent. Hence large eddies are directly resolved while small eddies are modeled. To perform the simulation with LES method in CFD are used the continuity and momentum equation, below are present the continuity and momentum equations without filtering.

$$\frac{\partial\rho}{\partial t}+\frac{\partial(\rho u_i)}{\partial x_i}=0 \quad (9)$$

$$\frac{\partial}{\partial t}(\rho u_i)+\frac{\partial}{\partial x_j}(\rho u_i u_j)=-\frac{\partial p}{\partial x_i}+\frac{\partial}{\partial x_j}\left[\rho\nu(\frac{\partial u_i}{\partial x_j}+\frac{\partial u_j}{\partial x_i})\right] \quad (10)$$

Filtering operation is applied to continuity and momentum equations

$$\frac{\partial\rho}{\partial t}+\frac{\partial(\rho\bar{u}_i)}{\partial x_i}=0 \quad (11)$$

$$\frac{\partial}{\partial t}(\rho\bar{u}_i)+\frac{\partial}{\partial x_j}(\rho\overline{u_i u_j})=-\frac{\partial\bar{p}}{\partial x_i}+\frac{\partial}{\partial x_j}\left[\rho\nu(\frac{\partial\bar{u}_i}{\partial x_j}+\frac{\partial\bar{u}_j}{\partial x_i})\right] \quad (12)$$

To reduce the momentum filter equation are used the following considerations :

1. The product of filter velocities is $\overline{u_i u_j}=\bar{u}_i\bar{u}_j+\bar{u}_i{}'\bar{u}_j{}'$;
2. The subgrid stress tensor, which is the Reynolds stress tensor is $\tau_{ij}{}'=\rho u_i{}' u_j{}'=\rho(\overline{u_i u_j}-\bar{u}_i\bar{u}_j)$;
3. The filtered strain tensor rate is $\bar{S}_{ij}=\frac{1}{2}\left(\frac{\partial\bar{u}_i}{\partial x_j}+\frac{\partial\bar{u}_j}{\partial x_i}\right)$;

4. The filtered viscous stress tensor is $\bar{\tau}_{ij} = 2\rho\nu\bar{S}_{ij}$.

The result of the reduction of the momentum filter equation is :

$$\frac{\partial}{\partial t}(\rho\bar{u}_i) + \frac{\partial}{\partial x_j}\left(\rho\overline{u_i u_j}\right) = -\frac{\partial\bar{p}}{\partial x_i} + \frac{\partial}{\partial x_j}(\bar{\tau}_{ij} - \tau_{ij}{}') \quad (13)$$

Spectrum of turbulent eddies in the Navier-Stokes equations is filtered :

- The filter is a function of grid size;
- Eddies smaller than the grid size are removed and modeled by a subgrid scale (SGS) model;
- Larger eddies are directly solved numerically by the filtered transient N-S equation.

Leonard (1974) proposes a model it as the application of a convolution filter to the exact solution. The filtered part $\bar{u}$ of the variable u is defined by the following convolution operator (denoted by the symbol * hereafter) :

$$\bar{u}(x,t) = \int_{-\infty}^{t}\int_{-\infty}^{+\infty} G\left(\bar{\Delta},\bar{\theta},|x-x'|,t-t'\right)u(x',t')dx'dt' = G(\bar{\Delta},\bar{\theta}) * u(x,t) \quad (14)$$

where $G\left(\bar{\Delta},\bar{\theta},|x-x'|,t-t'\right)$ is the kernel of the filter. The two arbitrary parameters $\bar{\Delta}$ and $\bar{\theta}$ are the cutoff length and the cutoff time, respectively. It can be proven that *G* must depend on the distance $|x-x'|$ to preserve certain symmetries of the Navier–Stokes equations. The small-scale subgrid part $u'$is then defined as :

$$u'(x,t) = u(x,t) - \bar{u}(x,t) \quad (15)$$

Next it is generated a filtration to reduce them for Explicit LES and Implicit LES:

- **Explicit** (i.e., associated with the application of a convolution filter to the DNS solution).
- **Implicit** (i.e., imposed by numerical errors, the computational mesh, or modeling errors) or even a blending of these two possibilities. The numerical filter: the numerical error, which is not uniformly distributed over the resolved frequencies, can also be interpreted as a filter. When local numerical methods such as finite element, finite volume, or finite difference methods are used to solve the governing equations, the numerical error is observed to be an increasing function of the wave number. Consequently, the dynamics of the highest frequencies resolved on the computational grid are only poorly captured, and these scales can be considered as being filtered.(M. Hahn et al , 2005),(Thornber et al, 2008) and (Drikakis et al. ,2009).

  The subgrid stress tensor is expressed as: $\tau'_{ij} = \rho(\overline{u_i u_j} - \bar{\bar{u}}_i\bar{\bar{u}}_j + \tilde{\tau}'_{ij})$, where the tensor $\tilde{\tau}'_{ij}$ is considered equal to subbgrid dissipation scale action.

High-resolution methods are most commonly associated with compressible flow solutions. Their introduction to incompressible flow solutions was most directly impacted by their use with a projection method by Bell, Colella, and Glaz (1989), as well as with the artificial compressibility method by Drikakis, Govatsos, and Papantonis (1988). (FERNANDO F. GRINSTEIN, LEN G. MARGOLIN, WILLIAM J. RIDER, 2007)

6 Domain Generation Methodology

The geometrical parameters of the cavity model in paper are displayed in Figure 7 (a- baseline Cavity geometry and b- wavy cavity geometry) are taken from the computational domain of Garry Hughes and Laurent Dala (Garry, Dala,2009),

Figure 7 Cavity geometry

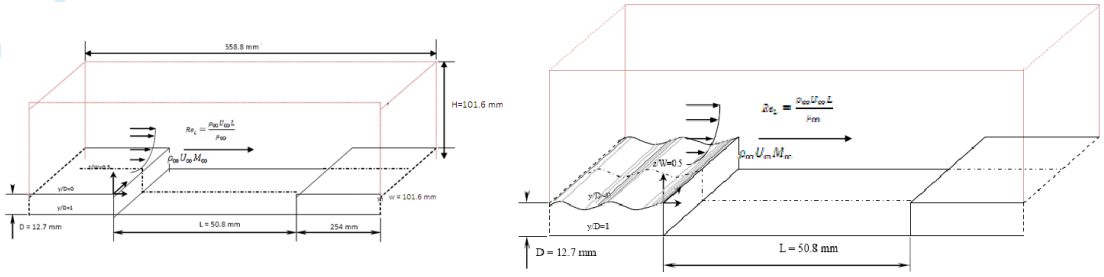

a- Baseline cavity dimensions **b- Wavy cavity dimensions**

Different surface modifications were simulated by varying the amplitude and frequency of surface waviness was constructed using **OpenFOAM** stands for (Open Source Field Operation And Manipulation) is an open source software package for CFD, which is produced by a commercial company, OpenCFD. The software package can be seen as a C++ library that provides two kinds of applications, solvers and utilities. Solvers are designed to solve a specific problem in continuum mechanics, whereas utilities are performing data manipulation tasks. For users with knowledge in programming, it is possible to add new solvers and utilities or modify the existing ones in order to fit the desired purpose.

We employ a large time-step transient solver in OpenFOAM toolbox for incompressible flow using PIMPLE (merged PISO-SIMPLE) algorithm. In order to work with OpenFOAM, the user needs to be familiar with the file structure. Figure 8.

Figure 8: File structure of OpenFOAM

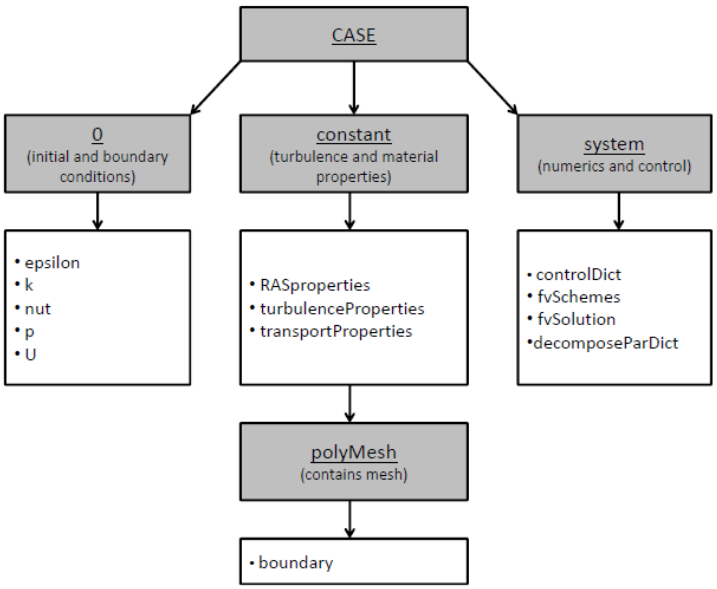

This solver makes it possible to dynamically adjust the time step in runtime based on the specified maximum Courant-Friedrichs-Lewy number, which reduces the initial relaxation time. The time discretization is performed by the implicit

Crank-Nicolson scheme with a coefficient of 0.5. The Gaussian-type schemes are chosen for the spatial (gradient, divergence, and laplacian) discretization. The Poisson equation for pressure is solved by GAMG (Generalized Geometric-Algebraic Multi-Grid) algorithm, while the linear equation for velocity is solved by PBiCG algorithm (Preconditioned Bi-Conjugate gradient solver for asymmetric matrices). Linear interpolation is used to obtain the physical quantities at the surface centers of the cells.

Figure 9 Schematic diagram of the computational domain

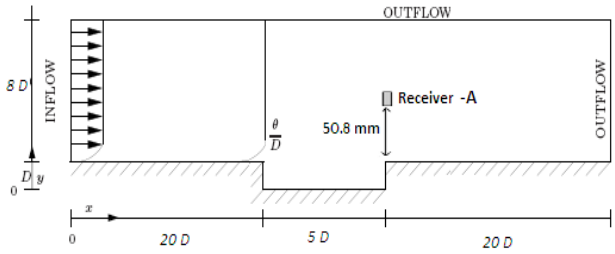

Table 2. Details of the Geometry

Total length of the domain	558.8 mm
Height of the domain	101.6 mm
Cavity length L	50.8 mm
Cavity depth D	12.7 mm
Aspect ratio of the cavity L/D	4

All simulations were performed on the cavity of aspect ratio $L/D=4$. Throughout the work, the length of the cavity is maintained as 50.8 mm and depth of the cavity as 12.7 mm. Figure 9 illustrates the schematic diagram of two dimensional domain adopted to simulate cavity flows. The flow is from left to right hand side. The domain extends between $0 \le x/D \le 45$ and $-1 \le y/D \le 8$. The computational domain extends to 20D and 20D upstream and downstream of the cavity leading and trailing edges, respectively, the sound signals are received on receiver-A. The Table 2 summaries the details related to the geometry of the two dimensional cavity.

6.1 Computational Mesh

The mesh is a very important part of the calculation; in the evaluation of a CFD simulation it is necessary to improve the mesh to generate a good simulation. To do that some dimensionless number are used:

Figure 10 and Table 3 shows the computational domain and the grid structure for the cavity. The following figure and table are respectively a scaled sketch of the cavity section and sub-divided into blocks with labeled edges and table of the meshing parameters associated to the different edges.

Figure 10: Side View of the Meshing Domain Sub-divided Into Four Blocks with Labeled Edges

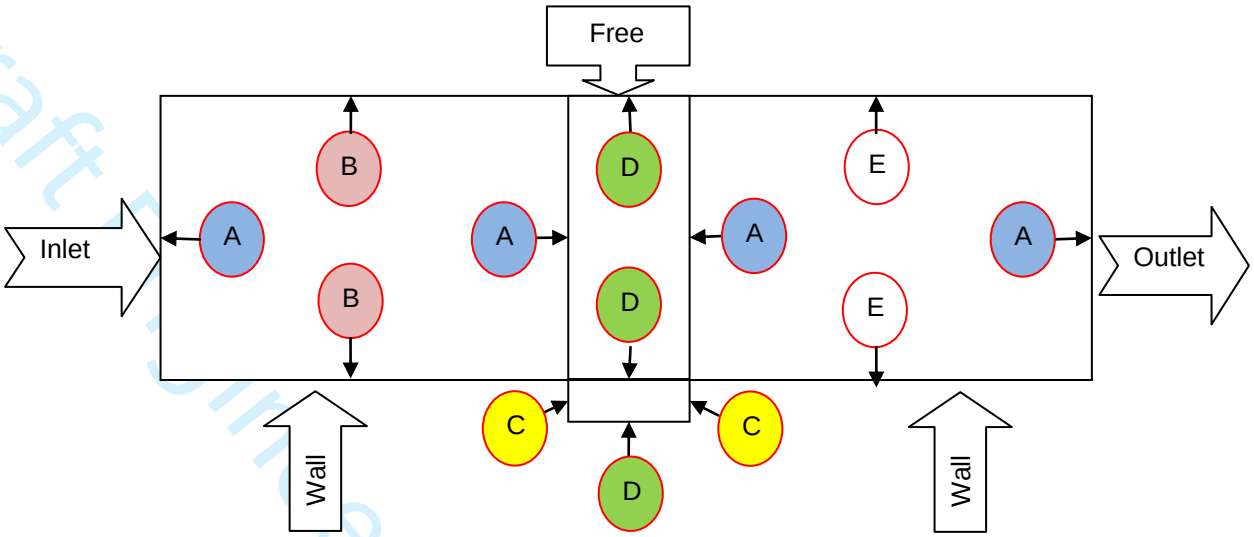

Table 3. Meshing Parameters

Edges	A	B	C	D	E	
Nodes	101	254	150	150	88	
grid size	72192					
Mesher Type	quadrilateral mesh					
y-plus	$y^+ = \frac{\sqrt{\frac{\tau_\omega}{\rho}}y}{\nu}$				y^+_{max}	117
					y^+_{mean}	0.2
Omega	$\Omega = \frac{NE}{ND} = \frac{Number\ of\ elements}{Number\ of\ nodes}$				0.99	
Courant-Friedrichs-Lewy (CFL)	$C = \frac{u_x \Delta t}{\Delta x} + \frac{u_y \Delta t}{\Delta y}$				C_{max}	0.59
					C_{mean}	0.09

For applications with complex, inhomogeneous flows and flow-induced noise radiation, the most promising and commonly used numerical technique is to adopt a hybrid approach. In such an approach, the sound-generation and sound-propagation processes are considered separately. The general idea is to alternate as fast as possible between a “noise generation” fine mesh criteria to a “noise propagation” coarser one. This is achieved by making sure that the highly turbulent zones are meshed with the fine criteria.

6.2 Initial and boundary conditions

Free stream variables for each length-to-depth ratio were set everywhere in the domain as the initial condition for the unsteady flow with M = 0.3 and $Re = 3.2\ 10^{-5}$. The results presented here were normalized on the following conditions: Air at 20 $°C$ and 1 bar; Dynamic viscosity $\mu = 1.82 \times 10^{-5}\ N\ s\ m^{-2}$, Density $\rho = 1.19\ kg\ m^{-3}$,

The boundary conditions are defined in the Table 4

Table 4: Boundary conditions of the

Boundary	Type	Value
Inlet	Free-stream	timeVaryingUniformFixedValue; M=0.3
Outlet	Pressure Outlet	zeroGradien
Cavity and bottom	Wall	No – Slip smooth
Top	Free- stream	zeroGradient

Furthermore, time dependency is a crucial factor of this study due the unsteadiness of the flow field consisting of random and periodic pressure fluctuation occurring within the cavity. Each time step was set as 0.25×10^{-5} seconds with initial time equal to zero and a the maximum time duration was set as 49500 time steps, cumulating a simulation time of 0.4975 seconds.

Figure 11 shows the density of mesh resolution near the walls and in the cavity region. The boxed region which is highlighted at the upper left corner represents the high mesh density. It is the region where the shear layer and other important mechanisms begin for hydrodynamics and aeroacoustics.

Figure 11 Mesh density: a) Baseline cavity b) Wavy cavity

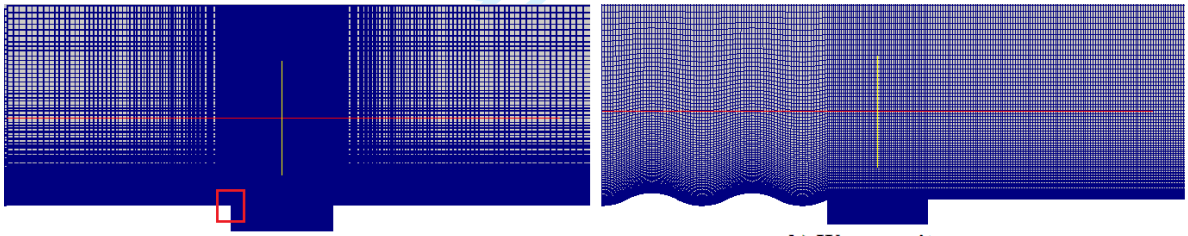

a) Baseline cavity b) Wavy cavity

7 Results

7.1 Aerodynamics

When a shear layer passes a cavity, it mainly keeps flowing downstream but the rest comes into the cavity and forms a recirculating flows. The predictions of instantaneous velocity flow field from **LES** simulations are shown in Figure 12.

Figure 12 Instantaneous flow field from LES simulations

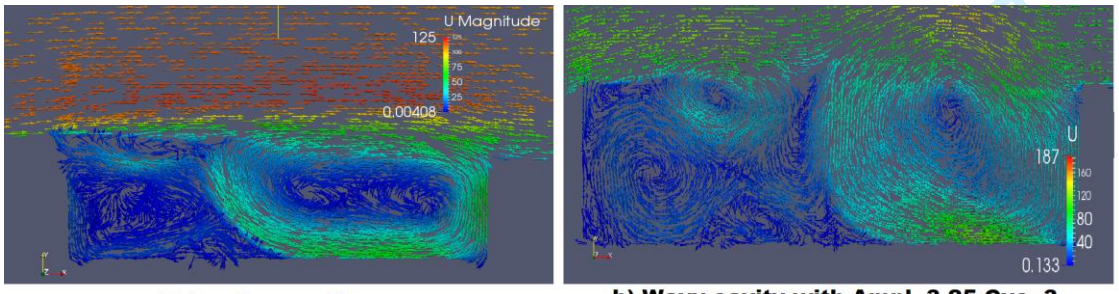

a) Baseline cavity b) Wavy cavity with Ampl. 3.25 Cyc. 3

Shear Mode

The test case (Ampl. 0 Cyc. 0) oscillates in shear mode. Figure 13 illustrates instantaneous vorticity contours in the cavity flow-field at different flow time after 60 computational periods.

The turbulent boundary layer which separates from the leading edge of cavity forms an oscillating shear layer. Figure 13-(a) shows the shear layer stretching from the upstream of the cavity and is parallel to the bottom of the cavity. Over the right upper corner of the cavity, shear layer with a tongue like structure extends to the downstream of the cavity from the vortex near to the vertical wall of the cavity. Figure 13-(b) describes the complex interaction between the shear layer and the vortex at the downstream wall of the cavity. The incoming shear layer extends until the middle of the cavity region and the lip of the shear layer swipes on the vertical wall at the trailing edge of the cavity. (The swiping action cuts the tongue like shear layer to travel downstream of the cavity.)

The shear layer which extends due to the oscillation, impinges on the upper right corner of cavity and breaks into two (see Figure 13-(c)) and at time period 3T/4 i.e in the Figure 13-(d), one part of the lip of the broken shear layer enters the cavity creating a eddy close to the downstream wall with the size of cavity depth, while the other part of the shear layer moves downstream of the cavity with less energetic eddies.

Figure 13 Instantaneous vorticity contours in the baseline cavity.
(a) 60.25T; (b) 60.5T; (c) 60.75T (d) 70T

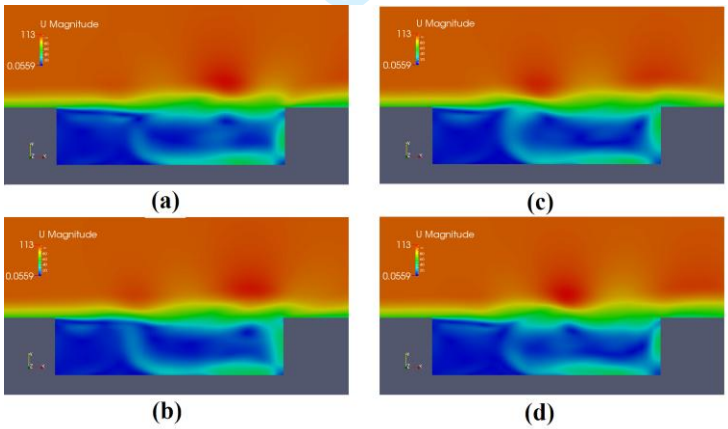

Wake Mode

Figure 14 shows the instantaneous vorticity fields U over a period. A vortex is formed from the trailing edge and fills the cavity region is shown in Figure 14-(a). In Figure 14-(b), the vortex detaches and impinges on the downstream corner of the cavity. Due to the impingement, is ruptured and moves out of the cavity, while another eddy enter the cavity from the leading edge of the cavity (see Figure 14-(c)). The eddy which is broken at this point of time moves downstream of the cavity, while another new eddy grows to fill the cavity is shown in the Figure 14-(d). The flow above the cavity region is affected by the flow from the cavity.

Figure 14 Instantaneous vorticity fields U for wake mode at four different times (a-d) corresponding to approximately a quarter of a period of oscillations. Only a small portion of the computational domain near the cavity is shown

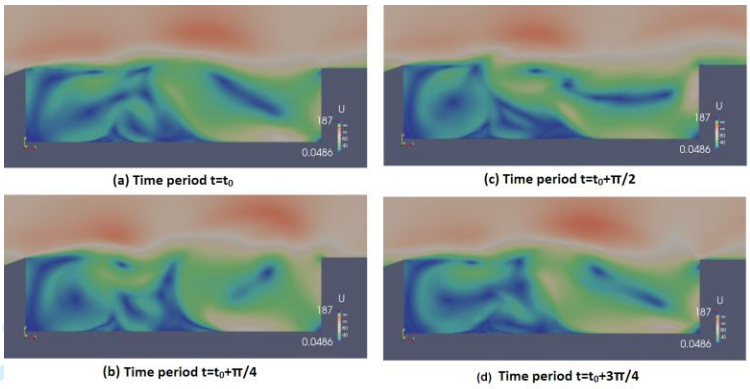

7.2 AeroAcoustic

Acoustic Parameters: The pressure perturbations p' ($p' = p - p_0$) which propagate as waves and which can be detected by the human ear. The Sound Pressure Level (SPL) is a logarithmic scale measure of the pressure unsteadiness in which the minimum pressure fluctuation detected by the human ear $p_{ref} = 2\times10^{-5} Pa$ is taken as the reference. For continuous pressure signals, the SPL is defined by:

$$SPL = 10\log(\frac{PSD}{p_{ref}}) \tag{16}$$

The PSD describes how the power of a signal or time series, in our case the time dependent pressure, is distributed with frequency. The PSD spectrum is determined by means of a Fast Fourier Transform (FFT) utilizing windowing as to smoothen the PSD estimate, in our case the Hanning window. The FFT of a signal P(t) is defined as $FFT(t,f) = \int_{-\infty}^{\infty} P(\tau)w(\tau - t)e^{-j2\pi f\tau}d\tau$ where $w(t)$ is the Hanning window function, applied to obtain a clear definition of the fundamental frequencies. Time averaging the pressure fluctuations one would obtain the mean pressure $\bar{P} = {}^{1}\!/_{N-N_0}\sum_{k=N_0}^{N} P_k(t)$ where N is the total number of samples taken and N_0 is the first sample number at which the time averaging starts. The root mean square pressure is therefore calculated via the equation $P_{rms} = {}^{1}\!/_{N-N_0}\sum_{k=N_0}^{N}\left(P_k(t) - \bar{P}\right)^2$.

Using the acoustic spectrum results, an overall sound pressure level (OASPL) can be obtained by adding all noise amplitudes of the spectrum, the OASPL can be obtained applying the following expression:

$$OASPL = 20log\sqrt{\sum_i (10^{SPL_i/20})^2} \tag{17}$$

Sound pressure levels (SPL) for the acoustic field above the cavity predicted by Rowley, et al (Rowley, 2002) and paper are shown in Figure 15, peak radiation to the far field occurs at an angle of about 135^0 from the downstream axis.

Figure 15 SPL distributions. (a) 2D-DNS predicted by Rowley, et al. (Rowley, 2002); (b) 2D-LES with surface wavy

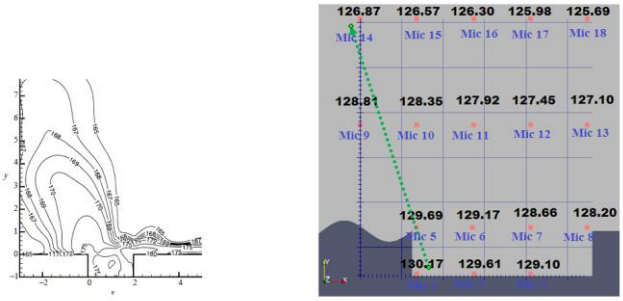

(a) (b)

Figure 16 shows the sound pressure level of the computed acoustic signal at Mach 0.3 (flow velocity 99.44 m/s). The spectral resolution of these results is 6.97 Hz. over the whole frequency range [0-10000] Hz. From the acoustic analysis it can be seen that the significant peak of the sound pressure level is at the frequency 2000 Hz correspond to the 2^{nd} Rossiter mode.

Figure 16 SPL at one receiver for baseline cavity

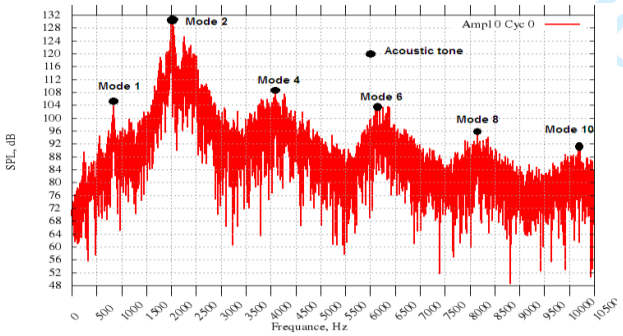

Table 5 Rossiter modal frequencies Wth associated Strouhal Numbers (Rossiter,1964)

m	St	f(Hz)
1	0.412	807.60
2	0.962	1884.39
3	1.512	2961.19
4	2.068	4037.98
5	2.612	5114.78
6	3.163	6191.57
7	3.713	7268.37
8	4.263	8345.16
9	4.813	9421.96
10	5.363	10498.75

The highest sound pressure level at this frequency is 129 dB (for receiver A, Figure 9). The peaks at 840 Hz, 2000 Hz, 4080 Hz, 6122 Hz, 80150 HZ and 10300 HZ correspond very well to the results predicted by Rossiter, Eqn. (1). (see Table 5). It is seen that in Figure 17-(a) the cavity for an applied surface waviness with frequency of $19.7x10^{-3}$ and $11.8x10^{-3}$ cycles per mm increase the resonance peak by 9 dB compared to the baseline case and also the peak of the sound pressure level is at the frequency 1000 Hz correspond to the 1^{st} Rossiter mode for wake mode.

Figure 17 Sound pressure level with and without surface waviness

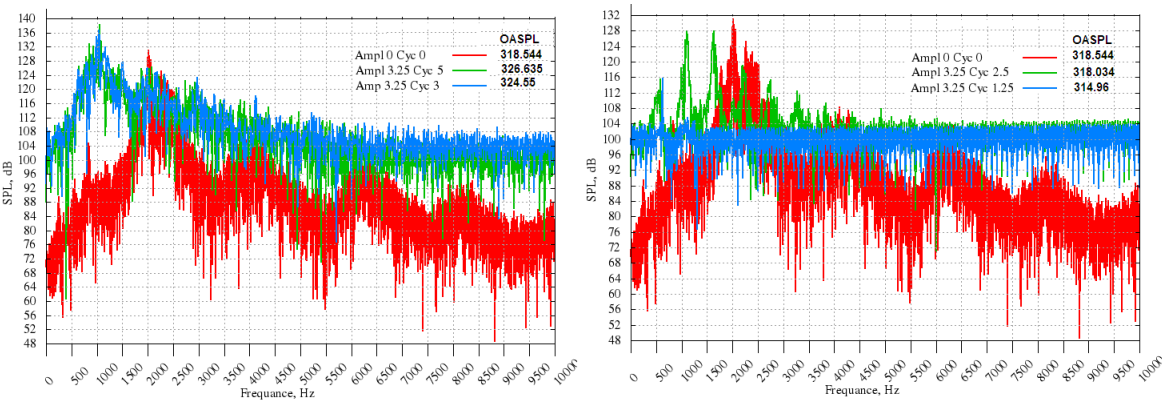

Figure 18 shows frequencies of the two most energetic peaks in the spectra for the series of run with $L/D = 4$, compared to experimental data and predictions from Eqn. (1), the transition to wake mode oscillations for M > 0.3.

Figure 18 Strouhal numbers for peaks in spectra for the shear-layer mode and wake modes

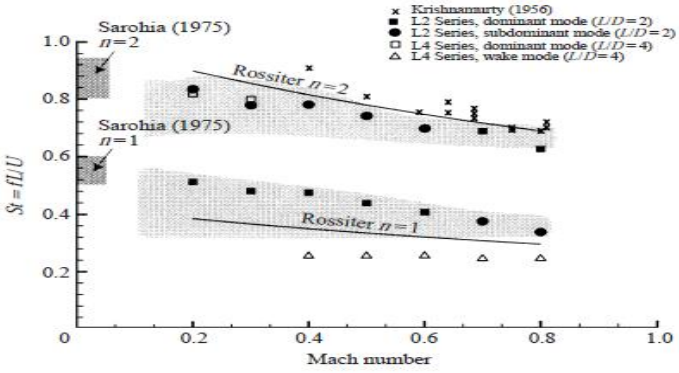

The results for surface wavy control, Figure 17-(b), show a considerable attenuation of the dominant Rossiter peak, it was clarified that the tonal sound reduced for frequency of 4.92×10^{-3}, 9.84×10^{-3} cycles per mm. The maximum noise level of 116 dB was observed at f= 625 Hz for frequency 4.92×10^{-3} cycles per mm and the maximum noise level of 127.8 dB was observed at f = 1095 Hz for frequency 9.84×10^{-3} cycles per mm. It was observed that the attenuation achieved using this configuration was of the highest value, giving an overall reduction in SPL of 14 dB. The comparison of the numerical simulation with the experimental measurements for acoustic part has not been carried out yet. But this study proves the influence of the surface wavy in the attenuation or amplification of sound and its intensity.

8 Conclusions

A complete two-dimensional analysis of both the baseline and the modified configuration were carried out. Additionally the flow regime was demonstrated with success by the use of CFD flow visualisation.

The results of different geometry modifications applied to the leading edge of a cavity with length to depth ratio of 4, in order to reduce the resonance of flow at Mach 0.3 have been presented. The amplitude of 3.25 mm and the frequency of $4.92x10^{-3}$ cycles per mm was observed as achieving the best reduction in cavity resonance.

Further Work

To fully understand the wavy surface impact on the cavity flow control, the following further work is required:

- Applying the used control mechanism on a range of Mach numbers is needed to further verify the effectiveness of the control system;
- Increasing the mesh density and study the influence on accuracy of the results;
- Using Implicit Large Eddy Simulation method (ILES) (Drikakis et al. ,2009);
- Wind Tunnel testing of an optimum 2D model.

Acknowledgments

The Computations were performed on the Al-Farabi Cluster computer of the Ecole Nationale Polytechnique Oran - MAURICE AUDIN.

References

Ahuja, K.K., Mendoza, J., (1995), "Effects of cavity dimensions, boundary layer, and temperature on cavity noise with emphasis on benchmark data to validate computational aeroacoustic codes".

Bilanin, A.J., Covert., E.E. (1973), "Estimation of possible excitation frequencies for shallow rectangular cavities". AIAA, 11:347 351.

Colonius, T., Lele, S. K., (2004), "Computational aeroacoustics: progress on nonlinear problems of sound generation". Progress in Aerospace Sciences 40,6:345 416, August 2004.

Curle., N. (1955), "The influence of solid boundaries upon aerodynamic sound".

Dix, R. E., Bauer, R. C., (2000), "Experimental and predicted acoustic amplitudes in a rectangular cavity". AIAA, 2002-0472.

Drikakis, D. et al. (2009), "Large Eddy Simulation Using High Resolution and High Order Methods", Philosophical Transactions Royal Society A, 367, 2985-2997.

Fernando F., Len G., William J. (2007) "Implicit Large Eddy Simulation: computing turbulent fluid dynamics" ISBN-13 978-0-511-53974-9 eBook (EBL) www.cambridge.org/9780521869829, Cambridge University Press 2007.

Fox, J., (1968), "A criterion for the transition between flow regimes in turbulent cavity flow". 4:364–365.

Gharib, M., Roshko, A. (1987), "The effect of flow oscillations on cavity drag". Fluid Mech, 177:501–530.

Hahn, M. et al. (2005), "Large eddy simulation of compressible turbulence using high-resolution methods". International Journal for Numerical Methods in Fluids, 47, 971-977.

Heller, H.H., Bliss, D.B (1975), "The physical mechanism of flow induced pressure fluctuation in cavities and concepts for their suppression". AIAA, pages 75–491.

Heller, H.H., Holmes, DG., COVERT, E.E., (1971), "Flow-induced pressure oscillations in shallow cavities". Sound Vib., 18:545–553.

Hughes, G., Mamo, T., Dala L. (2009), "Use of active surface waviness for control of cavity acoustics in subsonic flows". 15 th AIAA/CEAS Aeroacoustics Conference (30th AIAA Aeroacoustics Conference), Miami ,Florida, AIAA-2009-3202, May 2009.

Krishnamurty, K., (1955), "Acoustic radiation from two-dimensional flow in rectangular cutouts in aerodynamic surfaces". Naca Technical, TN 3487.

Leonard, A. (1974): Energy cascade in large-eddy simulations of turbulent fluid flows, Advances in Geophysics A, 18:237–248.

Lighthill, M.J (1952), "On sound generated aerodynamically the royal society of london".

Plentovich, E. (1992) "Three-dimensional cavity flow fields at subsonic and transonic speeds". Fluid Mech, TP-3358, 1992.

Plentovich, E. B., Stallings, R. L., Tracy, M. B., (1993), "Experimental cavity pressure measurements at subsonic and transonic speedsstatic-pressure results". TP-3358.

Rockwell, D., Knisely, C. (1980), "Vortex-edge interaction: Mechanisms for generating low frequency components". Phys. Fluids, 23(2):239/240, 1980.

Roshko, A. (1955), "Some measurements of flow in a rectangular cutout". 3488.

Rossiter, J.E., (1964), "Wind-tunnel experiments on the flow over rectangular cavities at subsonic and transonic speeds". Aeronautical Research Council Reports and Memoranda, Technical Report 3438.

Rowley,C.W., Colonius, T., (2002), "On self-sustained oscillations in two-dimensional compressible flow over rectangular cavities". Journal of Fluid Mechanics., 315:346, 455.

Sarohia., (1975), "Experimental and analytical investigation of oscillations in flows over cavities". PhD thesis.

Srinivisan, S., Baysal, O., (1991), "Navier-stokes calculations of transonic flow past cavities". Fluid Engineering, 113:369–376, September 1991.

Stallings, R., Wilcox, F. (1987), "Experimental cavity pressure distributions at supersonic speeds". NASA-TP-2683, June 1987.

Thornber, B., et al. (2008), "Implicit Large Eddy Simulation of a Deep Cavity Using High-Resolution Methods". AIAA Journal, Vol. 46, 10, 2634-2685.

Tracy, M. B., Plentovich, E., (1992), "Measurements of fluctuating pressure in a rectangular cavity in transonic flow at high Reynolds number". NASA TM 4363, TP-3358.

Symbols

D - Cavity Depth

L - Cavity Length

δ - Boundary layer thickness

f - Acoustic frequency of disturbance

f_m - Frequency of the m^{th} mode

p' - Pressure perturbations

p_{rms} - Root mean square pressure

R_e - Reynolds number

St - Strouhal number

P_{ref} - P_{ref} =2x10^{-5} Pa, The value adopted as the minimum audible sound pressure variation

Acronyms and Abbreviations

SPL - Sound Pressure Level

PSD - Power Spectral Density

OASPL - Overall Sound Pressure Level

FFT - Fast Fourier Transform

OpenFOAM - Open Field Operation And Manipulation

CFD - Computational Fluid Dynamics

.